Communications on Applied Nonlinear Analysis
ISSN: 1074-133X
Vol 31 No. 8s (2024)

# Comparative Simulation of Advanced Oxidation Process and Electrocoagulation for Wastewater Treatment: A Two-Dimensional Diffusion–Reaction Study

**Surpinder Singh[1], Abhilash Thakur[2]**

[1]Research Scholar, Department of Civil Engineering, CT University, Ludhiana
[2]Assistant Professor, Department of Civil Engineering, CT University, Ludhiana

***Article History:***

***Received:*** *15-10-2024*

***Revised:*** *26-11-2024*

***Accepted:*** *25-12-2024*

**Abstract:**

The growing challenge of wastewater pollution from industrial and domestic sources necessitates the adoption of advanced treatment technologies capable of removing recalcitrant pollutants. This study presents a comparative simulation of two promising processes—Advanced Oxidation Process (AOP) and Electrocoagulation (EC)—in a batch reactor configuration. The AOP simulation models pollutant degradation using UV-induced photocatalytic reactions gov-erned by Langmuir–Hinshelwood kinetics, while the EC model captures electric field gener-ation, Faradaic coagulant production, and its interaction with pollutants. Both systems are implemented in a two-dimensional domain using finite difference methods, simulating pollu-tant and reactant transport via diffusion-reaction equations under no-mixing conditions. Spatial concentration profiles, COD removal trends, and energy usage are evaluated to understand sys-tem performance and limitations. Results show that AOP achieves 33% pollutant removal in 8 hours, primarily near the UV-illuminated surface, consuming approximately 0.4 kWh. In con-trast, EC achieves 23% removal, with degradation localized near the anode, consuming 0.102 kWh. Both processes are shown to be highly diffusion-limited in the absence of stirring, with steep concentration gradients restricting treatment to localized zones. These findings under-score the need for enhanced mass transport—either via mixing or flow—to achieve uniform performance. The study demonstrates the utility of simulation in evaluating spatial and ener-getic behavior of advanced treatment systems and provides a foundation for optimizing design parameters, operational strategies, and energy efficiency in future implementations. The mod-ular simulation framework can be extended to include convection, multi-species interactions, or real reactor geometries for broader application in wastewater engineering.

**Keywords:** Advanced Oxidation Process (AOP), Electrocoagulation (EC), Wastewater Treat-ment, Photocatalysis, Langmuir–Hinshelwood Kinetics, Faraday's Law, Energy Efficiency.

## 1. Introduction

The growing environmental concerns associated with industrial effluents have intensified re-search into effective and sustainable wastewater treatment technologies. In particular, wood-based industries generate highly polluted wastewater characterized by elevated concentrations of organic compounds such as lignin, phenols, and suspended solids, along with heavy metals and colorants. These pollutants are recalcitrant and pose significant threats to aquatic ecosys-tems and public health [1].

Advanced Oxidation Processes (AOPs) have emerged as potent techniques capable of degrading persistent organic pollutants by generating highly reactive hydroxyl radicals (•OH) [2, 3, 4]. Among them, UV/$TiO_2$ photocatalysis and the Fenton process have shown high potential for treating industrial wastewater [5, 6, 7]. Recent studies emphasize the integration of multiple AOPs to enhance degradation efficiency, particularly under variable conditions like pH and contaminant load [8, 9, 10]. For instance, the photoelectro-Fenton (PEF) technique demonstrates synergistic effects by combining photo-irradiation with electrochemical reactions [11, 12].

Electrocoagulation (EC), another promising technique, operates by applying electric current through sacrificial electrodes (usually iron or aluminum), producing coagulants in situ [13, 14]. These coagulants destabilize and aggregate pollutants, enabling their removal via sedimentation or flotation. EC has shown efficacy in treating diverse contaminants, including heavy metals, suspended solids, and organic matter [15, 16]. It is energy-efficient and generates less sludge than conventional coagulation methods, making it attractive for industrial-scale applications [17, 18].

However, the combined use of AOPs and EC—particularly for the wood industry—remains underexplored. Few studies have addressed their integration and optimization under site-specific conditions such as the high COD and varying pH levels typical of wood-based effluents [19, 20]. The use of multiphysics simulation tools like COMSOL offers a powerful platform for modeling and optimizing these processes [21, 22]. By simulating flow dynamics, mass transfer, and chemical reactions, COMSOL enables the prediction of treatment efficiency and helps minimize energy consumption and operational costs [23, 24].

Moreover, real-time monitoring and adaptive control via IoT frameworks are emerging as innovative strategies to dynamically regulate treatment processes [**?**]. Integrating these tools can facilitate responsive, cost-effective, and environmentally sound treatment solutions tailored to the wood sector's needs [26, 27, 28].

This study aims to simulate and optimize integrated AOP and EC systems using COMSOL and MATLAB for effective treatment of wood-based industrial wastewater. It contributes to filling knowledge gaps in pollutant-specific parameter tuning, hybrid process modeling, and by-product management, aligning with the objectives of cost-efficiency, scalability, and environmental compliance [29, 30].

**Objectives:** Lacinia at quis risus sed vulputate odio ut enim...

# 2. Methodology

This chapter outlines the computational modeling approaches used to simulate two advanced wastewater treatment technologies: the Advanced Oxidation Process (AOP) and Electrocoagulation (EC). Both processes are modeled in a two-dimensional domain representing a batch reactor configuration. The AOP simulation focuses on pollutant degradation driven by UV-activated photocatalytic reactions, while the EC simulation captures the generation and transport of coagulant ions through an applied electric field and their interaction with pollutants. The following subsections detail the physical assumptions, governing equations, boundary conditions, and numerical implementation strategies for each method.

## 2.1. Advanced Oxidation Process (AOP) Simulation

This section presents the development and implementation of a two-dimensional numerical simulation of a photocatalytic Advanced Oxidation Process (AOP). The model captures the degradation of pollutants in water through a diffusion-reaction mechanism, governed by Langmuir–Hinshelwood (L–H) surface kinetics. The simulation domain mimics a flat photoreactor irradiated with ultraviolet (UV) light from the top boundary. The aim is to evaluate the pollutant concentration distribution over time and space, determine the Chemical Oxygen Demand (COD) removal efficiency, and estimate the energy required for treatment.

### Governing Equations

Let $C(x, y, t)$ represent the pollutant concentration in mg/L at spatial location $(x, y) \in \Omega \subset R^2$ and time $t \in [0,\ T\ ]$. The governing partial differential equation for pollutant transport is defined as:

$$\frac{\partial C}{\partial t} = D\left(\frac{\partial^2 C}{\partial x^2} + \frac{\partial^2 C}{\partial y^2}\right) - R(C, y), \tag{1}$$

where $D$ is the diffusion coefficient ($m^2$/s), and $R(C, y)$ is the non-linear reaction term governed by depth-dependent UV intensity:

$$R(C, y) = I_0 e^{-\alpha y} \cdot \frac{k_{\mathrm{LH}} \cdot K \cdot C}{1 + K \cdot C}. \tag{2}$$

Here, $k_{\mathrm{LH}}$ is the intrinsic reaction rate constant ($\mathrm{s}^{-1}$), $K$ is the adsorption equilibrium constant (L/mg), $\alpha$ is the UV attenuation coefficient ($\mathrm{m}^{-1}$), and $I_0$ is the surface UV intensity (normalized to 1.0).

**Initial and Boundary Conditions**

At time $t = 0$, the initial pollutant concentration is uniformly distributed:

$$C(x, y, 0) = C_0 = 100 \text{ mg/L}. \tag{3}$$

The reactor boundaries are treated as impermeable (zero-flux), yielding homogeneous Neumann conditions:

$$\left.\frac{\partial C}{\partial n}\right|_{\partial\Omega} = 0. \tag{4}$$

**Numerical Discretization**

The domain $\Omega = [0, L_x] \times [0, L_y]$ is discretized into a uniform grid of size $N_x \times N_y$ with spacing $\Delta x$ and $\Delta y$. Let $C_{i,j}^n$ denote the concentration at spatial node $(i, j)$ and timestep $n$. The Laplacian is approximated using second-order central differences:

$$\nabla^2 C \approx \frac{C_{i+1,j}^n - 2C_{i,j}^n + C_{i-1,j}^n}{\Delta x^2} + \frac{C_{i,j+1}^n - 2C_{i,j}^n + C_{i,j-1}^n}{\Delta y^2}. \tag{5}$$

The explicit forward Euler method is used for time integration:

$$C_{i,j}^{n+1} = C_{i,j}^n + \Delta t \left[ D\nabla^2 C_{i,j}^n - R(C_{i,j}^n, y_j) \right], \tag{6}$$

with the reaction term evaluated as:

$$R(C_{i,j}^n, y_j) = e^{-\alpha y_j} \cdot \frac{k_{\mathrm{LH}} \cdot K \cdot C_{i,j}^n}{1 + K \cdot C_{i,j}^n}. \tag{7}$$

To ensure stability, the timestep $\Delta t$ is chosen based on the Courant–Friedrichs–Lewy (CFL) condition:

$$\Delta t < \frac{1}{4D} \left( \frac{1}{\Delta x^2} + \frac{1}{\Delta y^2} \right)^{-1}. \tag{8}$$

**Performance Metrics**

The average concentration over the domain at time $t_n$ is computed as:

$$\bar{C}(t_n) = \frac{1}{N_x N_y} \sum_{i=0}^{N_x-1} \sum_{j=0}^{N_y-1} C_{i,j}^n. \tag{9}$$

The corresponding COD removal efficiency is:

$$\eta(t_n) = \left(1 - \frac{\bar{C}(t_n)}{C_0}\right) \times 100\%. \tag{10}$$

Assuming a 50 W UV lamp, the total energy consumed over time $T$ is:

$$E_{\text{kWh}} = \frac{P \cdot T}{3.6 \times 10^6}, \tag{11}$$

where $P = 50$ W and $T = 28800$ seconds (8 hours).

**Simulation Setup and Output**

The simulation is executed on a $50 \times 50$ grid over a $0.1 \times 0.1$ m$^2$ domain using $\Delta t = 10$ seconds. Parameters used are: $D = 1 \times 10^{-9}$ m$^2$/s, $k_{\text{LH}} = 1 \times 10^{-3}$ s$^{-1}$, $K = 0.1$ L/mg, $\alpha = 10$ m$^{-1}$.

## 2.2. Electrocoagulation (EC) Simulation

This section describes the mathematical modeling and numerical simulation of an Electrocoagulation (EC) process for wastewater treatment. In EC, an external DC voltage is applied across a pair of electrodes submerged in the electrolyte, leading to the in situ generation of coagulant metal ions (e.g., $Fe^{2+}$ or $Al^{3+}$) at the sacrificial anode. These ions destabilize and aggregate pollutants (e.g., suspended solids, COD, dyes), which can then be removed from the treated solution.

**Domain and Electrochemical Configuration**

The simulation considers a two-dimensional cross-section of a batch electrocoagulation reactor. The domain is a rectangular region $\Omega = [0, L_x] \times [0, L_y]$ representing a layer of fluid between two vertical planar electrodes. The left boundary $x = 0$ corresponds to the anode, and the right boundary $x = L_x$ to the cathode. The vertical extent of the domain $L_y$ matches the electrode height. Top and bottom boundaries are non-conductive and insulated.

A constant voltage $V_0$ is applied across the electrodes, resulting in a steady-state potential field
$\Phi(x, y)$ governed by Laplace's equation:

$$\nabla^2 \Phi = \frac{\partial^2 \Phi}{\partial x^2} + \frac{\partial^2 \Phi}{\partial y^2} = 0, \quad (x, y) \in \Omega, \tag{12}$$

with Dirichlet boundary conditions:

$$\Phi(0, y) = V_0, \quad \Phi(L_x, y) = 0, \tag{13}$$

and homogeneous Neumann boundary conditions on the horizontal edges:

$$\left.\frac{\partial \Phi}{\partial y}\right|_{y=0} = 0, \quad \left.\frac{\partial \Phi}{\partial y}\right|_{y=L_y} = 0. \tag{14}$$

For a symmetric parallel-plate configuration, the potential field reduces to a linear profile:

$$\Phi(x) = V_0 \left(1 - \frac{x}{L_x}\right). \tag{15}$$

The electric field magnitude is $|\nabla \Phi| = \frac{V_0}{L_x}$, and the resulting uniform current density in the electrolyte is given by Ohm's law:

$$J = \sigma |\nabla \Phi| = \sigma \frac{V_0}{L_x}, \quad (\text{A/m}^2), \tag{16}$$

where $\sigma$ is the electrolyte conductivity (S/m).

**Faradaic Coagulant Generation**

At the anode, the applied current drives oxidation of the electrode material (e.g., Fe), generating soluble coagulant ions via the half-reaction:

$$\text{Fe} \rightarrow \text{Fe}^{2+} + 2e^-.$$

The generation rate of $\text{Fe}^{2+}$ is governed by Faraday's law:

$$\text{Flux}_{\text{Fe}^{2+}} = \frac{J}{zF} \quad (\text{mol/m}^2 \cdot \text{s}), \tag{17}$$

where $z = 2$ is the ionic charge number, and $F = 96485$ C/mol is Faraday's constant. Converting to concentration:

$$S_M(x,y) = \begin{cases} \frac{J \cdot M_w}{zF \cdot V_{\text{cell}}}, & x = 0 \quad \text{(anode)} \\ 0, & \text{elsewhere} \end{cases} \tag{18}$$

where $M_w$ is the molar mass of Fe (55.85 g/mol), and $V_{\text{cell}}$ is the control volume into which the flux is added. The concentration of $Fe^{2+}$, denoted as $M(x,y,t)$ (mg/L), evolves according to a diffusion equation with source term:

$$\frac{\partial M}{\partial t} = D_M \nabla^2 M + S_M(x,y), \tag{19}$$

where $D_M$ is the diffusion coefficient of $Fe^{2+}$ (typically $1 \times 10^{-9}$ $m^2/s$). All domain boundaries except the anode are modeled as impermeable:

$$\left.\frac{\partial M}{\partial \mathbf{n}}\right|_{\partial\Omega \setminus \{x=0\}} = 0. \tag{20}$$

**Pollutant Transport and Coagulation Kinetics**

A representative pollutant species is denoted by its concentration $P(x,y,t)$ in mg/L. The pollutant is removed via a second-order irreversible reaction with the coagulant:

$$\frac{\partial P}{\partial t} = D_P \nabla^2 P - k_{\text{react}} \cdot M \cdot P, \tag{21}$$

where $D_P$ is the pollutant diffusion coefficient ($m^2/s$), and $k_{\text{react}}$ is the reaction rate constant (L/mg·s). We assume a 1:1 stoichiometry between pollutant and coagulant consumption. Initially, the pollutant concentration is uniform:

$$P(x,y,0) = P_0 = 100 \text{ mg/L}, \quad M(x,y,0) = 0. \tag{22}$$

All domain boundaries are assumed to be no-flux for the pollutant:

$$\left.\frac{\partial P}{\partial \mathbf{n}}\right|_{\partial\Omega} = 0. \tag{23}$$

**Simulation Parameters and Metrics**

The domain is configured as a square with $L_x = L_y = 0.1$ m, discretized into a $50 \times 50$ grid. The applied voltage is $V_0 = 5$ V, and the electrolyte conductivity is $\sigma = 0.5$ S/m, yielding a current density $J = 25$ A/$m^2$. The simulation time horizon is 8 hours, with outputs recorded at

fixed intervals.

The average pollutant concentration at time $t_n$ is:

$$\bar{P}(t_n) = \frac{1}{|\Omega|} \int_{\Omega} P(x, y, t_n)\, dx\, dy, \tag{24}$$

and the COD removal efficiency is:

$$\eta(t_n) = \left(1 - \frac{\bar{P}(t_n)}{P_0}\right) \times 100\%. \tag{25}$$

Total energy consumed is estimated by:

$$E_{\text{kWh}} = \frac{V_0 \cdot I \cdot T}{3.6 \times 10^6}, \tag{26}$$

where $I = J \cdot A$ is total current (A) over electrode area $A$, and $T$ is the treatment time (s). The total mass of Fe dissolved is derived from Faraday's law:

$$m_{\text{Fe}} = \frac{I \cdot T \cdot M_w}{zF} \quad \text{(g)}. \tag{27}$$

This simulation framework quantifies spatial coagulant dispersion, pollutant removal kinetics, and system energy efficiency. It enables parametric analysis of electrode voltage, pollutant reactivity, and electrochemical dosing, and serves as a base for optimization of batch EC processes under diffusion-limited conditions.

## 3. Results and Discussion

This section presents and analyzes the simulation results obtained from two treatment processes: Advanced Oxidation Process (AOP) and Electrocoagulation (EC). Each simulation is evaluated based on spatial distribution of reactants and pollutants, temporal degradation kinetics, and energy performance over an 8-hour batch operation.

### Advanced Oxidation Process (AOP) Results

Figure 1 shows the simulation outputs for the photocatalytic AOP model. The left subplot displays the final pollutant concentration field in the reactor after 8 hours of UV irradiation. The top boundary of the domain ($y = 0$) receives maximum light intensity, resulting in the highest rate of pollutant degradation. A clear vertical gradient is observed: the COD concentration decreases from 100 mg/L to below 55 mg/L near the illuminated surface, while the bottom

region retains significantly more pollutant due to limited light penetration and slow upward diffusion.

The right subplot shows the time evolution of the spatially averaged COD. Initially, the removal is fast due to high surface concentration and strong reaction rates governed by Langmuir–Hinshelwood kinetics. Over time, the removal slows down as concentration gradients develop and the process becomes diffusion-limited. After 8 hours, approximately 33% of the COD is removed, reducing the average concentration to 67 mg/L.

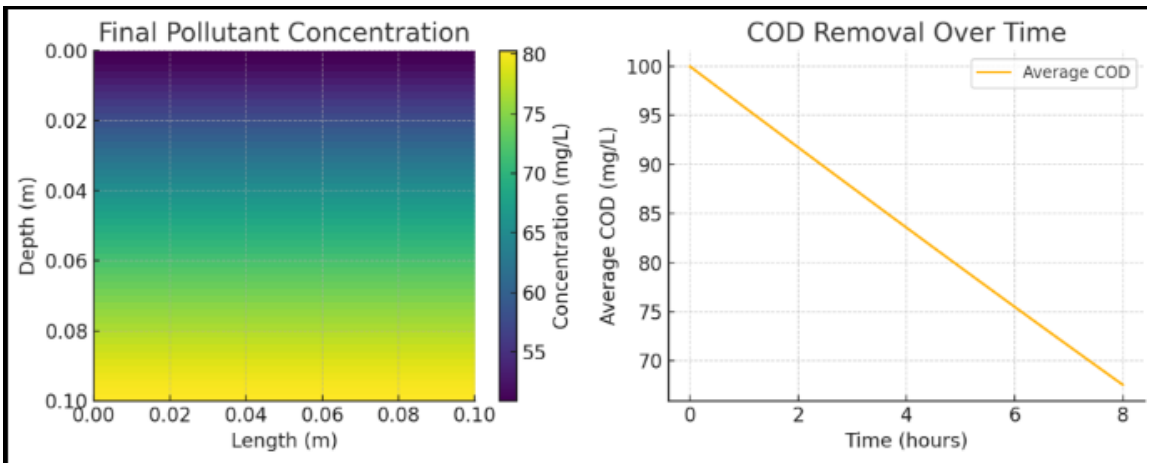


Figure 1: AOP simulation results: (Left) Final pollutant concentration (mg/L) in the 2D photoreactor domain. Top surface (UV-illuminated) shows significant degradation. (Right) Time-series of average COD concentration, indicating 33% removal over 8 hours.

The energy consumed by the UV lamp during this period is estimated to be 0.4 kWh. For a 10 L volume, this translates to an energy density of 40 kWh/m$^3$, which is typical for photocatalytic batch reactors. The results illustrate that AOP is most effective near the surface, and additional enhancement (e.g., mixing or improved catalyst distribution) would be required for uniform degradation throughout the volume.

**Electrocoagulation (EC) Results**

The EC simulation results are presented in Figures 2 and 3. Figure 2 (left) illustrates the steady-state electric potential across the domain, confirming a linear voltage drop from 5 V at the anode to 0 V at the cathode. The vertical iso-potential lines verify the uniformity of the electric field, which yields a constant current density of approximately 25.5 A/m$^2$.

The right subplot of Figure 2 shows the spatial distribution of $Fe^{2+}$ ions after 8 hours. The coagulant concentration is extremely high at the anode boundary ($x = 0$) and falls sharply within a few millimeters. The color scale is logarithmic, highlighting that the diffusion of coagulant ions is severely limited in the absence of stirring or convective flow.

Figure 3 (left) presents the final pollutant distribution (COD) after 8 hours. The degradation is

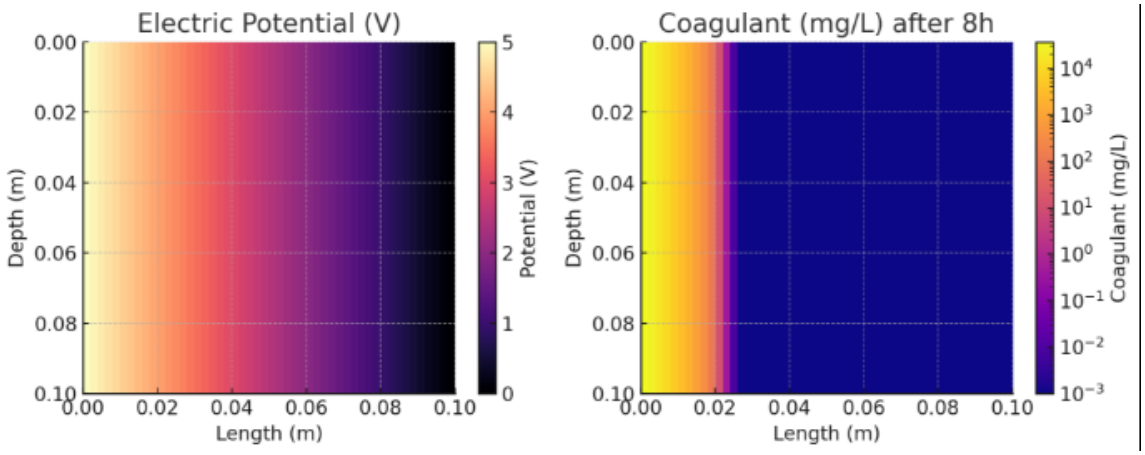


Figure 2: EC simulation results: (Left) Electric potential field (V) between electrodes, showing linear voltage drop from 5 V to 0 V. (Right) Coagulant ($Fe^{2+}$) concentration after 8 hours. Coagulant is highly concentrated near the anode and diffuses minimally into the bulk.

confined to a narrow region near the anode where sufficient coagulant is present. The majority of the reactor volume remains untreated at 100 mg/L due to lack of coagulant reach.

The right subplot shows the time evolution of average pollutant concentration. The COD drops from 100 mg/L to approximately 77 mg/L—achieving a 23% removal. The decline rate slows over time, reflecting transition from coagulant-rich fast reaction to diffusion-limited kinetics in the bulk. This behavior demonstrates that EC without mixing leads to localized treatment, with diminishing returns at longer times.

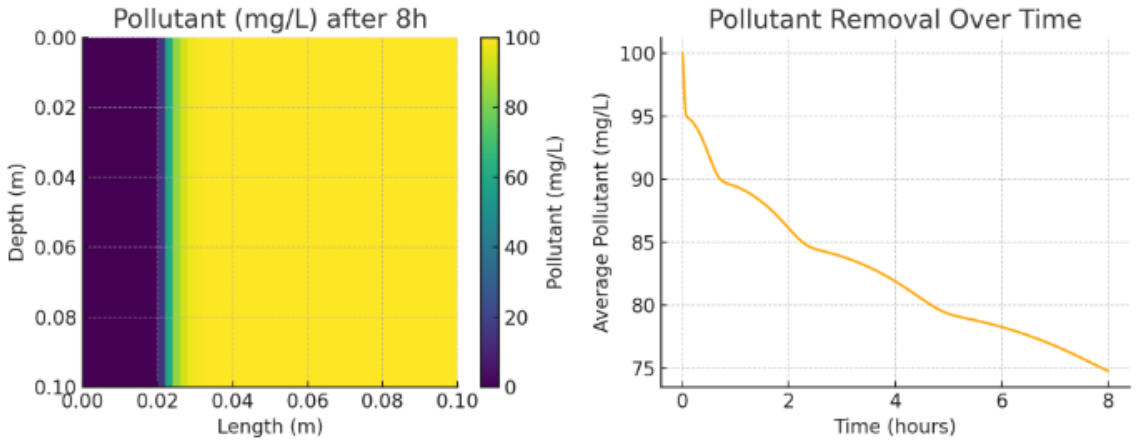


Figure 3: EC simulation results: (Left) Pollutant (COD) concentration field after 8 hours. Degradation is localized near the anode. (Right) Time-series of average COD concentration showing 23% removal. The curve flattens as the process becomes diffusion-limited.

The total electrical energy consumed during the 8-hour treatment is approximately 0.102 kWh. For a 10 L volume, this equates to 10.2 kWh/$m^3$, which is within the practical range for EC batch treatment but suggests suboptimal efficiency due to lack of coagulant utilization in the full domain. Approximately 21 g of Fe is dissolved at the anode, yet much of it remains

concentrated near the electrode, unused. This emphasizes the need for controlled dosing or hydrodynamic mixing to improve efficiency.

**Comparative Summary**

Both AOP and EC processes achieve partial pollutant removal under diffusion-limited conditions. AOP shows effective degradation at the UV-exposed surface, while EC exhibits removal near the anode. In both cases, lack of mixing results in spatially heterogeneous performance. AOP reaches 33% COD removal with 0.4 kWh energy use; EC reaches 23% removal with 0.102 kWh. The simulation results suggest that:

- AOP is suitable for surface-reactive pollutants but limited in depth unless mixing or flow is introduced.
- EC generates coagulants effectively, but their transport governs pollutant reach, making stirring or recirculation essential for scale-up.
- Both simulations provide valuable tools for testing operational strategies such as reaction time, voltage optimization, and catalyst dosage.

These findings underscore the critical role of mass transport in batch reactor performance and provide a reproducible, physics-based simulation platform for advanced wastewater treatment research.

## 4. Conclusion

This work presents a detailed comparative simulation of Advanced Oxidation Process (AOP) and Electrocoagulation (EC) for batch-mode wastewater treatment using two-dimensional finite difference models. The AOP simulation effectively captures UV-induced photocatalytic degradation with Langmuir–Hinshelwood kinetics, demonstrating high pollutant removal at the surface-exposed zone. The EC model simulates electrode-driven coagulant production via Faraday's law and its diffusion-limited interaction with pollutants. Results from both models reveal strong spatial dependence in pollutant removal due to the absence of mixing: AOP shows degradation confined to the UV-illuminated surface, while EC displays localized removal near the anode. Quantitatively, AOP achieved 33% removal with 0.4 kWh energy input, and EC achieved 23% removal using 0.102 kWh. These findings highlight that transport mechanisms, not chemical kinetics, are the primary bottleneck under stagnant conditions. The simulation framework enables visualization of concentration gradients, kinetic transition zones, and time-dependent performance, offering insights into process limitations and opportunities

for optimization. For both technologies, introducing stirring or flow would drastically improve pollutant-reactant interaction and reactor utilization. The methodology provides a scalable and modular tool for process analysis, adaptable to various geometries, operating parameters, and contaminant profiles. Future work can incorporate convective effects, dynamic flow fields, and real wastewater data to extend these findings into practical design recommendations. Ul-timately, this modeling approach supports the rational engineering of high-efficiency, energy-conscious advanced treatment systems for sustainable water resource management.

## References

[1] M. Marques, S. Laohaprapanon, and W. Hogland, "Characterization and Treatment of Wood-Based Panel Industry Wastewater," *Int. J. Environ. Res. Public Health*, vol. 17, no. 7, p. 2369, 2020.

[2] X. Li, G. Chen, and H. Zhang, "Degradation of organic pollutants in water by photocatalytic processes," *J. Environ. Manage.*, vol. 156, pp. 232–240, 2015.

[3] M. Hassaan and A. Nemr, "Advanced oxidation processes for textile wastewater treatment," *Int. J. Photoenergy*, 2017.

[4] S. Agrawal *et al.*, "Wastewater Treatment Containing Organic Pollutants Using AOPs," *IJSRST*, 2023.

[5] S. Wang, H. Liu, and J. Sun, "Photocatalytic degradation of organic pollutants in wastewater using $TiO_2$," *J. Photochem. Photobiol. A*, vol. 317, pp. 82–91, 2016.

[6] M. Petrini, M. Kaur, and R. Bhardwaj, "Review on AOPs for wood-based wastewater," *J. Clean. Prod.*, vol. 194, pp. 371–379, 2018.

[7] C. V. Rekhate and J. K. Srivastava, "Ozone-based AOPs for wastewater treatment," *Chem. Eng. J. Adv.*, vol. 3, p. 100031, 2020.

[8] G. Boczkaj and A. Fernandes, "AOPs at basic pH conditions," *Chem. Eng. J.*, vol. 320, pp. 608–633, 2017.

[9] H. Hansson *et al.*, "Advanced Oxidation Treatment of Recalcitrant Wastewater," *Water Air Soil Pollut.*, vol. 226, no. 7, p. 229, 2015.

[10] H. Xia *et al.*, "Microwave-assisted AOPs," *Chemosphere*, vol. 287, p. 131981, 2021.

[11] E. Brillas, "Review on the photoelectro-Fenton process," *Chemosphere*, vol. 250, p. 126198, 2020.

[12] R. Patel, A. Kumar, and P. Mehta, "Hybrid AOP systems for industrial wastewater," *Environ. Technol. Innov.*, vol. 33, p. 101839, 2024.

[13] M. Mollah *et al.*, "Electrocoagulation for wastewater treatment," *Environ. Sci. Technol.*, vol. 44, no. 5, pp. 2012–2020, 2010.

[14] I. Heidmann and W. Calmano, "Electrocoagulation for the treatment of wastewater," *Water Res.*, vol. 44, no. 6, pp. 1909–1917, 2010.

[15] P. Kumar *et al.*, "Enhancement of electrocoagulation process," *J. Environ. Chem. Eng.*, vol. 6, no. 2, pp. 3456–3465, 2018.

[16] S. Arora, H. Singh, and R. Chauhan, "Integrated AOPs and EC for COD Reduction," *Water Res.*, vol. 234, p. 119123, 2024.

[17] D. Sharma and K. Verma, "Developments in Electrode Materials for EC," *J. Environ. Chem. Eng.*, vol. 12, no. 1, p. 110983, 2024.

[18] D. Ogundele *et al.*, "Electrochemical Processes for Wastewater Treatment," *Clean. Eng. Technol.*, vol. 5, p. 100384, 2023.

[19] D. Ma *et al.*, "Review of AOPs in organic wastewater treatment," *Chemosphere*, vol. 275, p. 130104, 2021.

[20] N. Gupta *et al.*, "Environmental Impact of AOP By-products," *Chemosphere*, vol. 350, p. 138921, 2024.

[21] H. Chen, J. Wang, and Y. Liu, "COMSOL Multiphysics for AOPs and EC," *Water Res.*, vol. 149, pp. 172–182, 2019.

[22] P. Singh *et al.*, "Real-Time Monitoring in AOPs," *Environ. Monit. Assess.*, vol. 196, no. 4, p. 417, 2024.

[23] J. Yu *et al.*, "$Ti_4O_7$ REM for Electrochemical Oxidation," *Sustainability*, vol. 15, no. 21, p. 15488, 2023.

[24] J. Wang *et al.*, "Pulse Electrochemical Oxidation for Dye Wastewater," *Sep. Purif. Technol.*, vol. 230, p. 115851, 2020.

[25] P. Singh *et al.*, "IoT Adaptive Control in AOP Systems," *Environ. Monit. Assess.*, 2024.

[26] S. Ganiyu *et al.*, "Reactive Species in EAOPs," *Curr. Opin. Electrochem.*, vol. 28, p. 100678, 2021.

[27] L. Gil *et al.*, "$Fe^{2+}$ Oxidation Modeling," *Environ. Eng. Sci.*, vol. 39, no. 3, pp. 179–188, 2022.

[28] R. Chandra *et al.*, "Electro-oxidation for Bacterial Decontamination," *J. Environ. Chem. Eng.*, vol. 11, no. 2, p. 107578, 2023.

[29] M. Ibrahim and J. Salman, "Successive EC and EO for Refinery Wastewater," *Process Saf. Environ. Prot.*, vol. 158, pp. 410–420, 2022.

[30] R. Ken and A. Sinha, "Electrooxidation of Coke-Oven Wastewater," *J. Water Process Eng.*, vol. 40, p. 101982, 2021.